Journal of Neuroinflammation

RESEARCH

Open Access

Therapeutic reduction of neurocan in murine intracerebral hemorrhage lesions promotes oligodendrogenesis and functional recovery

Hongmin Li[1,2,3], Samira Ghorbani[2,4], Olayinka Oladosu[2], Ping Zhang[5], Frank Visser[2], Jeff Dunn[6], Yunyan Zhang[2], Chang-Chun Ling[5], V. Wee Yong[2*] and Mengzhou Xue[1*]

Abstract

Background Intracerebral hemorrhage (ICH) causes prominent deposition of extracellular matrix molecules, particularly the chondroitin sulphate proteoglycan (CSPG) member neurocan. In tissue culture, neurocan impedes the properties of oligodendrocytes. Whether therapeutic reduction of neurocan promotes oligodendrogenesis and functional recovery in ICH is unknown.

Methods Mice were retro-orbitally injected with adeno-associated virus (AAV-CRISPR/Cas9) to reduce neurocan deposition after ICH induction by collagenase. Other groups of ICH mice were treated with vehicle or a drug that reduces CSPG synthesis, 4-4-difluoro-*N*-acetylglucosamine (difluorosamine). Rota-rod and grip strength behavioral tests were conducted over 7 or 14 days. Brain tissues were investigated for expression of neurocan by immunofluorescence microscopy and western blot analysis. Brain cryosections were also stained for microglia/macrophage phenotype, oligodendrocyte lineage cells and neuroblasts by immunofluorescence microscopy. Tissue structural changes were assessed using brain magnetic resonance imaging (MRI).

Results The adeno-associated virus (AAV)-reduction of neurocan increased oligodendrocyte numbers and functional recovery in ICH. The small molecule inhibitor of CSPG synthesis, difluorosamine, lowered neurocan levels in lesions and elevated numbers of oligodendrocyte precursor cells, mature oligodendrocytes, and $SOX2^+$ $nestin^+$ neuroblasts in the perihematomal area. Difluorosamine shifted the degeneration-associated functional state of microglia/macrophages in ICH towards a regulatory phenotype. MRI analyses showed better fiber tract integrity in the penumbra of difluorosamine mice. These beneficial difluorosamine results were achieved with delayed (2 or 3 days) treatment after ICH.

Conclusion Reducing neurocan deposition following ICH injury is a therapeutic approach to promote histological and behavioral recovery from the devastating stroke.

Keywords Extracellular matrix, Neurocan, Chondroitin sulphate proteoglycans, Oligodendrogenesis, Functional recovery, Intracerebral hemorrhage

*Correspondence:
V. Wee Yong
vyong@ucalgary.ca
Mengzhou Xue
xuemengzhou@zzu.edu.cn
Full list of author information is available at the end of the article

Background

Intracerebral hemorrhage (ICH) is a crippling condition characterized by the sudden rupture of cerebral vessels and entry of blood into the brain parenchyma [1]. ICH constitutes 15 to 20% of all strokes [2], and is particularly catastrophic with a mortality rate of over 50% [3]. The pathophysiology of ICH is complex and consists of mechanical disruption, neuroinflammation and demyelination [4, 5]. Patients with ICH that survive the stroke recover some neurofunctional deficits several months after [2], suggesting reorganization or regeneration of neural elements. Indeed, signs of regeneration such as oligodendrogenesis are found in autopsied samples of people dying from ICH [6]. Thus, understanding what promotes or impedes regeneration processes, and overcoming impediments, may enhance recovery from ICH.

The extracellular matrix (ECM) is a complex network of molecules dispersed throughout the extracellular space of the CNS [7]. ECM components are normally expressed in the CNS at three discrete locations: around vessels where they constitute the dense basement membranes that help maintain the integrity of the blood–brain barrier, around the soma of certain neuronal populations where they are referred to as perineuronal nets, and between cells termed the neural interstitial matrix [8]. Upon injuries to the CNS, many ECM molecules are excessively deposited by immune cells and reactive astrocytes into lesions where they have been found to inhibit axonal regeneration [9], impede properties of OPCs and remyelination, and enhance neuroinflammation [10, 11]. While the reasons for ECM deposition after CNS injuries remain unclear, with attempts at reconstitution of the blood–brain barrier and other repair activities being postulated [7], their dysregulated and excessive accumulation result in the aforementioned detriments.

A major component of the ECM is the family of chondroitin sulphate proteoglycans (CSPGs). CSPGs are widely expressed in the CNS [8], but they accumulate in high amounts in lesions. An important subgroup of CSPGs is the lecticans that include 4 members: aggrecan, brevican, versican and neurocan [12]. After intraventricular hemorrhage in premature rabbit pups, levels of lectican CSPG members are elevated in the forebrain [13]. Lectican CSPGs enhance macrophage migration and production of pro-inflammatory cytokines including interleukin-6 and tumor necrosis factor-α [14, 15].

Much remains unknown of the accumulation of CSPGs in stroke [8]. We previously documented that amongst the lectican CSPGs, neurocan was selectively and profoundly elevated in both murine and human ICH [16]. In tissue culture, neurocan inhibited adhesion and process outgrowth of OPCs, which are early steps in myelination in vivo [10, 16, 17]. Thus, neurocan appears to be a candidate to overcome in order to improve regenerative processes in ICH.

In the current study, we aimed to address critical gaps of knowledge on the potential inhibitory effects of the elevated neurocan in ICH. First, we targeted neurocan genetically by reducing its level using adeno-associated virus (AAV) to determine its impact on regenerative processes. Next, for potential translation into the clinic, we tested per-*O*-acetylated 4,4-difluoro-*N*-acetylglucosamine (Ac-4,4-diF-GlcNAc, referred henceforth as difluorosamine), which we previously found to inhibit CSPG production [11], to determine whether this small molecule drug could enhance recovery from ICH in acute (7 days) and longer term (14 days) repair. Our results highlight therapeutic targeting of the brain ECM, and difluorosamine as a lead drug, to regain lost deficits from ICH.

Methods

Mice

All animal experiments were performed with ethics approval (protocol number AC21-0073) from the Animal Care Committee at the University of Calgary under regulations of the Canadian Council of Animal Care. For the majority of the experiments, male C57BL/6 wildtype mice aged 8 to 12 weeks were purchased from Charles River. For the study comparing between young versus old mice in response to ICH, we used CX3CR1^{CreER}:Rosa26^{TdT} (Ai9) mice that were bred in our colony; these mice were not used here for lineage tracing studies but rather because they were available in 2 divergent age groups. The mice were 6 or 52 weeks old at the time of the ICH injury. Mice were housed between 21 and 23 °C, in low humidity, with 12 h light and 12 h dark cycle from 7 am light and starting 7 pm dark, environmental enrichment and free access to food and water.

ICH induction

The protocol for induction has been described elsewhere [18]. In brief, 0.05 U of collagenase type VII dissolved in 0.5 µl of saline was injected at a rate of 0·1 µl/min over 5 min into the right striatum. The needle was maintained at the same spot for additional 5 min to prevent reflux. The mice were sutured and then monitored in a thermally controlled environment until recovery.

For difluorosamine treatment, mice were randomized into two groups of 6 mice on day of ICH induction. Intraperitoneal daily treatment with either difluorosamine (25 mg/kg, dissolved in saline) or vehicle (saline) was started from 2 days post onset of ICH in the 7-day experiment, or every 2 days intraperitoneal treatment starting from 3 days post onset of ICH in the 14-day experiment.

ICH brain tissue harvest

Mice were sacrificed at 7- or 14-days post-collagenase injection with a lethal dose of ketamine and xylazine. Animals were perfused with a total of 10 ml of phosphate-buffered saline (PBS) and 10 ml of 4% paraformaldehyde (PFA) in PBS via cardiac puncture. The whole brain was collected into 4% PFA in PBS for fixation overnight, and then was transferred into 30% sucrose solution for 72 h. The cerebellum was excised, and the remaining brain tissue was frozen in FSC 22 frozen section media (Leica). Brain blocks were cut coronally by a cryostat into 20 µm sections, collected onto microscope slides and stored at − 20 °C before staining.

Plasmid construction and AAV-CRISPR/Cas9 production

pJEP317-pAAV-U6SaCas9gNRA (SapI)-EFS-GFP-KASH-pA, pJEP312-pAAV-CMV-SaCas9-P2A-HAFLA-GHA-KASH-pA [gifts from Jonathan Ploski1 (Addgene plasmid # 113694) [19]; (Addgene plasmid # 113689)], and pAAV-GFP-eGFP [gift from Bryan Roth (Addgene plasmid # 50473)] were obtained from Addgene. The AAV vectors were manipulated to drive expression of GFP and SaCas9 specifically in glial cells. The EFS promoter of pJEP317-pAAV-U6SaCas9gNRA (SapI)-EFS-GFP-KASH-pA was removed by AgeI and Xba restriction enzyme digestion and replaced with the GFAP promoter sequence PCR amplified from pAAV-GFAP-GFP to generate pAAV-U6-GFAP-GFP-KASH-pA; this was done by the NEBuilder hifi DNA assembly cloning kit (New England Biolabs). Similarly, the CMV promoter of pJEP312-pAAV-CMV-SaCas9-P2A-HAFLAGHA-KASH-pA was excised by digestion with XbaI and AgeI and replaced with the GFAP promoter sequence PCR amplified from pAAV-GFAP-GFP to generate pAAV-GFP-SaCas9-P2A-HAFLAGHA-KASH-pA.

Potential single guide RNAs (sgRNAs) with the SaCas9 PAM sequence (NNGRR) targeting the mouse neurocan gene were designed using the Broad Institute CRISPick sgRNA algorithm [20, 21] using the cDNA sequence of NCAN (accession NM_007789.3). The top ranked sgRNA (5′-GATAATGGAACACGACGCCTG-3′), targeting the antisense strand of exon 4 was chosen. Complementary oligonucleotides with appropriate overhang sequences and 5′ phosphorylation modifications 5′-P-ACCGACCCTCCTGCATGACACTTCG-3′ and 5′-P-AACCGAAGTGTCATGCAGGAGGGTC-3′ were annealed and subcloned into BspQI-digested pAAV-U6-GFAP-GFP-KASH-pA to generate pAAV-U6Fblns-gRNA-GFP-KASH-pA. For the non-target control, sgRNA targeting lacZ, a sequence that does not occur in the mouse genome, (Gtgcgaatacgcccacgcgat) was used by subcloning the oligos 5′-P-ACC Gtgcgaatacgcccacgcgat-3′ and 5′-P-AACATCGCGTGGGCGTATTCGCAC-3′ into the BspQI site of pAAV-U6-GFAP-GFP-KASH-pA to generate pAAV-U6lacZsgRNA-GFAP-GFP-KASH-pA. All plasmid constructs were verified by restriction enzyme mapping and Sanger DNA sequencing.

To produce the AAVs, AAV viral vectors containing the PHP·eB capsid were generated following Challis et al. [22].

The indicated pairs of vectors encoding Cas9 under the control of a GFAP promoter and gRNA (NCAN specific or non-target control) were co-delivered by retro-orbital injection to 6- to 8-week-old WT C57BL/6J mice at 3×10^{11} vg/virus 2 weeks before ICH induction (Fig. 1A).

Antibodies

The primary and secondary antibodies used are displayed in Table 1.

Immunofluorescence staining

Microscope slides with brain tissues were thawed at room temperature for 30 min, then hydrated with PBS for 5 min, and permeabilized with 0.1% Triton X-100 in PBS for 5 min. Tissue sections were blocked by horse serum blocking solution (0.01 M PBS, 1% bovine serum albumin (BSA), 10% horse serum, 0.1% Triton-X100, 0.1% cold fish gelatin, and 0.05% Tween-20) for 1 h at room temperature. Alternatively, for staining using the CC1 antibody in mice, AffiniPure Fab fragment donkey

(See figure on next page.)

Fig. 1 AAV-mediated reduction of neurocan improves oligodendrogenesis and functional recovery in ICH mice. **A** The paradigm of AAV injection and subsequent experimental protocol. **B**, **C** Graphs comparing the latency of rota-rod test (**B**) or forelimb force of grip strength test (**C**) between control (Ctrl) and knockdown (KD) groups. **D** Representative confocal images from 7-day Ctrl (left) and KD (right) mice in perihematomal area, where the lower left corner inside the dotted lines in **D** is the lesion core. Scale bar = 50 µm. **E** Quantifications for neurocan percent area of the lesion region of interest (ROI), where each ROI is a region defined by area occupied by Iba1$^+$ cells (n = 8 mice). **F** Representative 3D reconstruction images of perihematomal area at day 7 in Ctrl (left) and KD (right) mice, and internal accumulation of neurocan (red) within individually labelled GFAP$^+$ cells. Scale bar = 8 µm. **G** Quantification showing the percentage of GFAP$^+$ cells containing neurocan molecules. **H** Representative confocal images of day 7 perihematomal areas. Scale bar = 50 µm. **I**–**K** Number of Olig2$^+$ cells (**I**), OPCs (olig2$^+$ PDGFRα$^+$) (**J**) or mature oligodendrocytes (**K**) per mm^2 of lesion ROI (mean ± SEM of 8 mice). Each dot represents mean of 4 locations per mouse. There were 8 mice per group, and this experiment was completed in one series. Unpaired two-tailed Student's *t*-test; ns: not significant. $^{**}p < 0.01$, $^{***}p < 0.001$, $^{****}p < 0.0001$

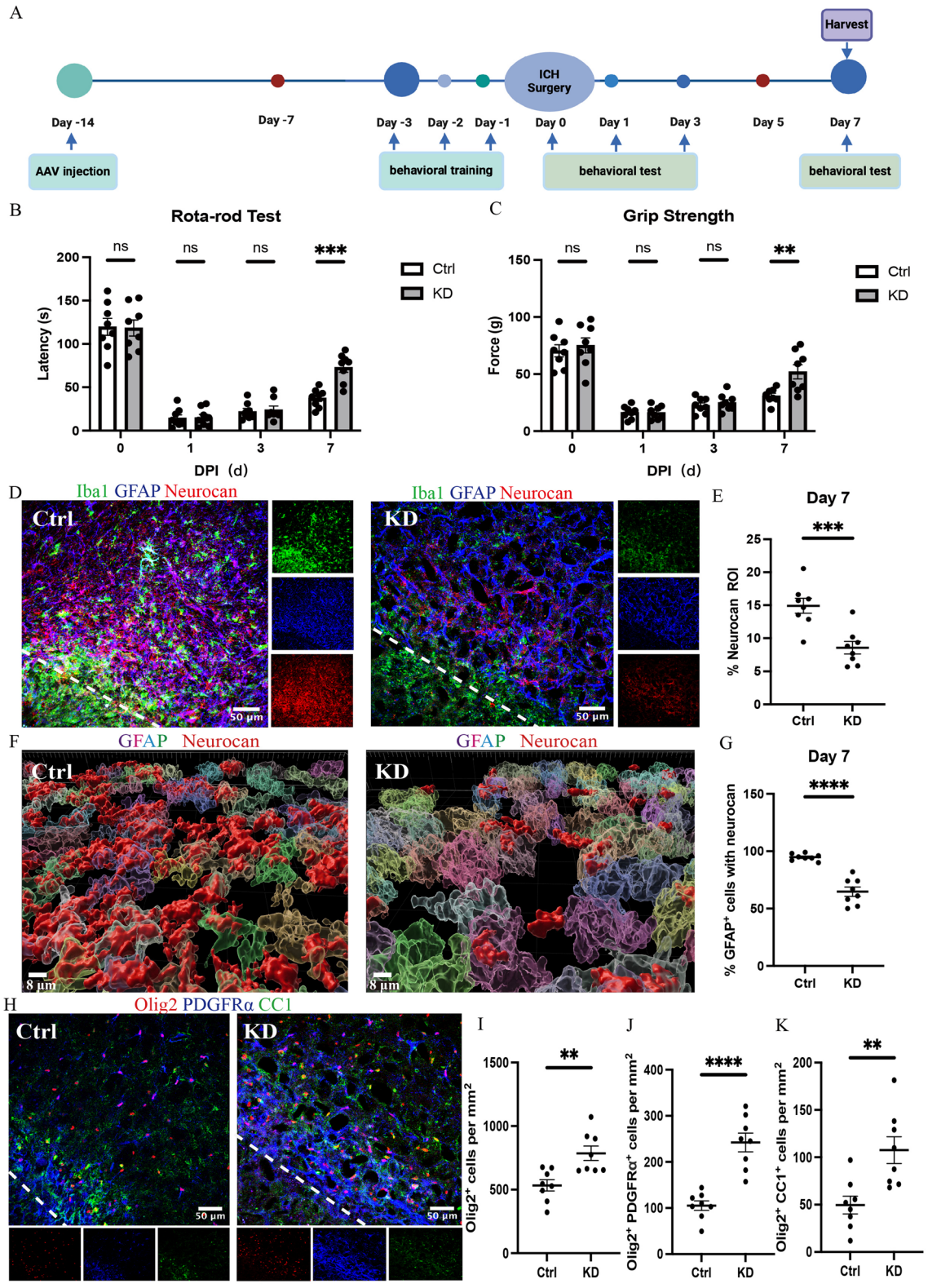

Fig. 1 (See legend on previous page.)

Table 1 Primary and secondary antibodies used in the current study

Target	Antibody	Commercial source	Catalog number	Dilution from supplier stock
Astrocytes	Chicken anti-mouse glial fibrillary acidic protein (GFAP)	BioLegend	829401	1:1000
Microglia/macrophages	Goat anti-human/mouse Iba1	ThermoFisher	PA5-18039	1:250
Microglia/macrophages	Goat anti-human/mouse Iba1	Wako	019-19741	1:1000
IL-1β	Goat anti-mouse interleukin IL-1β	R&D	AF-401-NA	1:50
Arg1	Rabbit anti-mouse arginase 1	Cell signalling	93668S	1:200
Neurocan	Rabbit anti-mouse neurocan	Millipore	ABT 1347	1:100
SOX2	rat anti-human/ mouse SOX2	ThermoFisher	14-9811-82	1:200
Nestin	chicken anti-human/mouse nestin	Novusbio	NB100-1604	1:1000
Ki67	rabbit anti-human/mouse Ki67	Abcam	AB15580	1:500
Clec7a	Rat anti-mouse Dectin-1	Invivogen	Mabg-mdect	1:100
Neurocan	Rabbit anti-mouse neurocan	Abcam	AB277525	1:1000
PDGFRα	Goat anti-mouse platelet-derived growth factor receptor	R&D	AF1062	1:200
Oligodendrocyte	Rabbit anti- human/mouse Olig2	Millipore	AB9610	1:200
CC1	Mouse anti-human/mouse adenomatous polyposis coli (APC)	Millipore	OP80-100UG	1:200
Rabbit IgG	Alexa Fluor 647 donkey anti-rabbit IgG	Jackson ImmunoResearch	711-605-152	1:400
Goat IgG	Alexa Fluor 488 donkey anti-goat IgG	Jackson ImmunoResearch	705-545-147	1:400
Mouse IgM	Alexa Fluor 488 donkey anti-mouse IgM	Jackson ImmunoResearch	715-545-140	1:400
Chicken IgY	Cyanine Cy3 donkey anti-chicken IgY	Jackson ImmunoResearch	703-165-155	1:400
Goat IgG	Cyanine Cy3 donkey anti-goat IgG	Jackson ImmunoResearch	705-165-147	1:400

anti-mouse IgG (H+L) (Jackson ImmunoResearch, 715-007-003, 1:50) was added to the blocking buffer. Tissues were incubated with primary antibodies suspended in antibody dilution buffer (0.01 M PBS, 1% BSA, 0.1% Triton-X100, 0.1% cold fish gelatin) overnight at 4 °C. Next, slides were washed three times with PBS containing 0.2% Tween-20 and incubated with fluorophore conjugated secondary antibodies (1:400) and 1 µg/ml of DAPI for 1 h. The slides were washed three times and mounted using Fluoromount-G solution (SouthernBiotech).

Western Blot

Lysates were loaded into sodium dodecyl sulphate (SDS) gels (NuPAGE 3–8% Bis–Tris Gel, Invitrogen) and ran with HiMark™ Pre-stained Protein Standard (Invitrogen) at 170 V for 1 h. The proteins were transferred using electroblotting to an 0.2 µm polyvinylidene fluoride membrane (PVDF) (GE Healthcare Life Science). The PVDF membrane was rinsed with tris-buffered saline (TBS) containing 0.05% Tween 20 (TBST) and blocked with 10% m/v skim powdered milk in TBS for 1 h at room temperature. A primary antibody of rabbit anti-mouse neurocan (1:1000; Abcam) or anti-fibronectin (1:500; Abcam) was added to 3% milk in TBS and incubated overnight at 4 °C. The membrane was washed five times (5-min/each) with TBST followed by incubation with secondary antibodies conjugated with horseradish peroxidase (HRP) for 1 h at room temperature. The membrane was washed five times (5 min each) with TBST before visualization using enhanced chemiluminescent (ECL) substrate (SuperSignal™ West Femto Maximum Sensitivity Substrate, Thermo Scientific) and imaged with the BioRad ChemiDoc system. To probe for β-actin, the membranes were washed using Restore™ Western blot stripping buffer (Thermo Scientific) for 30 min before blocking with 5% m/v BSA in TBS for 1 h at room temperature. The membrane was then incubated with primary antibody HRP anti-beta actin antibody (Abcam) in 3% m/v BSA in TBS for 1 h at room temperature before washing (5x/5 min each). The blots were visualized and imaged using the same methods as above, with quantification using the gel analyzer function in ImageJ. The relative amount of protein was normalized to actin.

Widefield and confocal fluorescence microscopy

Overviews of brain sections were imaged with an Olympus VS120 slide scanner using a 10×/0.4NA objective. These were used to locate the lesions. Only the

brightness and contrast were adjusted to better display representative images. All samples were then imaged on a Leica TCS SP8 laser scanning confocal microscope using a 25×/0.95 NA water objective. Three-dimensional (3D) z-stacks images (2048×2048×37 voxels) of the four fluorescent probes were acquired using the 405 nm, 488 nm, 552 nm, and 640 nm lasers sequentially at either 228×228×567 nm or 114×114×567 nm voxel size. The two different resolutions were used for quantifying % area of ECM molecules in Regions of Interest (ROIs) and % positive cells with ECM molecules, respectively. Imaging parameters were kept constant for each set of experiments.

Confocal image analysis

ImageJ software (NIH) was used to quantify the % ECM molecules in ROIs. For each z-stack image, maximum-intensity projections were created and ROIs were drawn around the perihematomal, lesion center, and contralateral areas according to GFAP or Iba1 labeling. Image segmentation was achieved using a set intensity threshold for each probe. Negative secondary antibody controls or contralateral controls were used to assess baseline signals and determine thresholds. For each probe, intensity threshold as well as size and circularity filters were kept constant across all samples for each experimental set. Total area and percent area (i.e., % ECM molecules in ROI) were measured.

Imaris software (Oxford Instruments) was used to determine the percentage of $Iba1^+$ or $GFAP^+$ cells overlapping with ECM molecules. Labelled areas were segmented as surfaces via a set intensity threshold determined as above. $Iba1^+$ or $GFAP^+$ cells were separated using seed points within the Imaris Surface creation workflow to obtain the total number of cells. For each probe, intensity threshold and surface details were kept constant within each set of experiments. % positive cells with ECM molecules were obtained by dividing the number of positive cells with ECM molecule by the total number of positive cells.

For better visualization of representative images shown, brightness and contrast were adjusted consistently across all samples and the images were converted to RGB.

Behavioral tests

Locomotor functions were evaluated before and 1, 3, 7, 14 days after ICH induction using rota-rod test and grip strength test. These tests were previously described [18]. Mice were transported to the testing room at least 30 min prior to training or testing to adjust to the environment before each session.

MRI imaging

MRI data were acquired using a 9.4T Bruker BioSpin equipped with a Bruker cryoprobe and operated with ParaVision V.5.1. Mice were anaesthetized initially with 2%–3% isoflurane and a tail vein cannulation were done before imaging. Mice were head-fixed in an animal carrier using tooth and ear bars. Anesthesia was maintained by 1.5% isoflurane. Respiration and body temperature were non-invasively monitored using a small animal monitoring system (Small Animal Instruments). Initially, a shimming procedure was conducted to correct the distortions and optimize the magnetic field homogeneity followed by a scout scan using a Gradient Echo sequence to determine the lesion epicenter and scan range. Subsequently, a T2-weighted FLASH sequence was acquired with 32 slices and 0.25 mm thickness using the following parameters: repetition time = 1500 ms, echo time = 6.5 ms, acquisition time = 25 min, flip angel = 90°, averages = 2, matrix size = 512×512; FOV = 19.2 mm×19.2 mm. Diffusion tensor imaging as a common advanced MRI method at the same location was implemented using an Echo Planar Imaging sequence and the following parameters: repetition time = 8000 ms, echo time = 35.66 ms, slice thickness = 0.5 mm, acquisition time = 37 min, averages = 2, FOV = 15 mm×15 mm, matrix size = 128×128; gradient duration = 4 ms, diffusion directions = 30 and b value = 3000 s/mm^2.

(See figure on next page.)

Fig. 2 Daily difluorosamine treatment for 5 days reduces neurocan and promotes functional recovery in ICH. **A** Chemical structure of difluorosamine. **B** Experimental paradigm. **C**, **D** Graphs comparing the latency of rota-rod (**C**) or forelimb force of grip strength (**D**) tests between control and DIF mice; each black circle is a different mouse across 3 separate experiments (n of 6, 6 or 8 in each of the experiment per group; N = 20 total). **E** Representative confocal images of perihematomal area (left) and lesion core (right) at day 7 in control and DIF mice stained for neurocan (red), Iba1(green), GFAP (blue). The lower left corner inside the dotted lines is the lesion core. Scale bar = 50 µm. **F** Bar graphs comparing the levels of neurocan in perihematomal area, lesion core and contralateral area at day 7 (N = 6). Data are mean ± SEM and analyzed by two-way ANOVA-Tukey's post hoc test. Western blot analysis (N of 4) of neurocan (**G**) and quantification (**H**) comparing the signal ratio of neurocan to β-actin among sham, control, and DIF mice; mean ± SEM, one-way ANOVA-Tukey's post hoc test; ns: not significant. Significance indicated as $^{**}p < 0.01$, $^{***}p < 0.001$

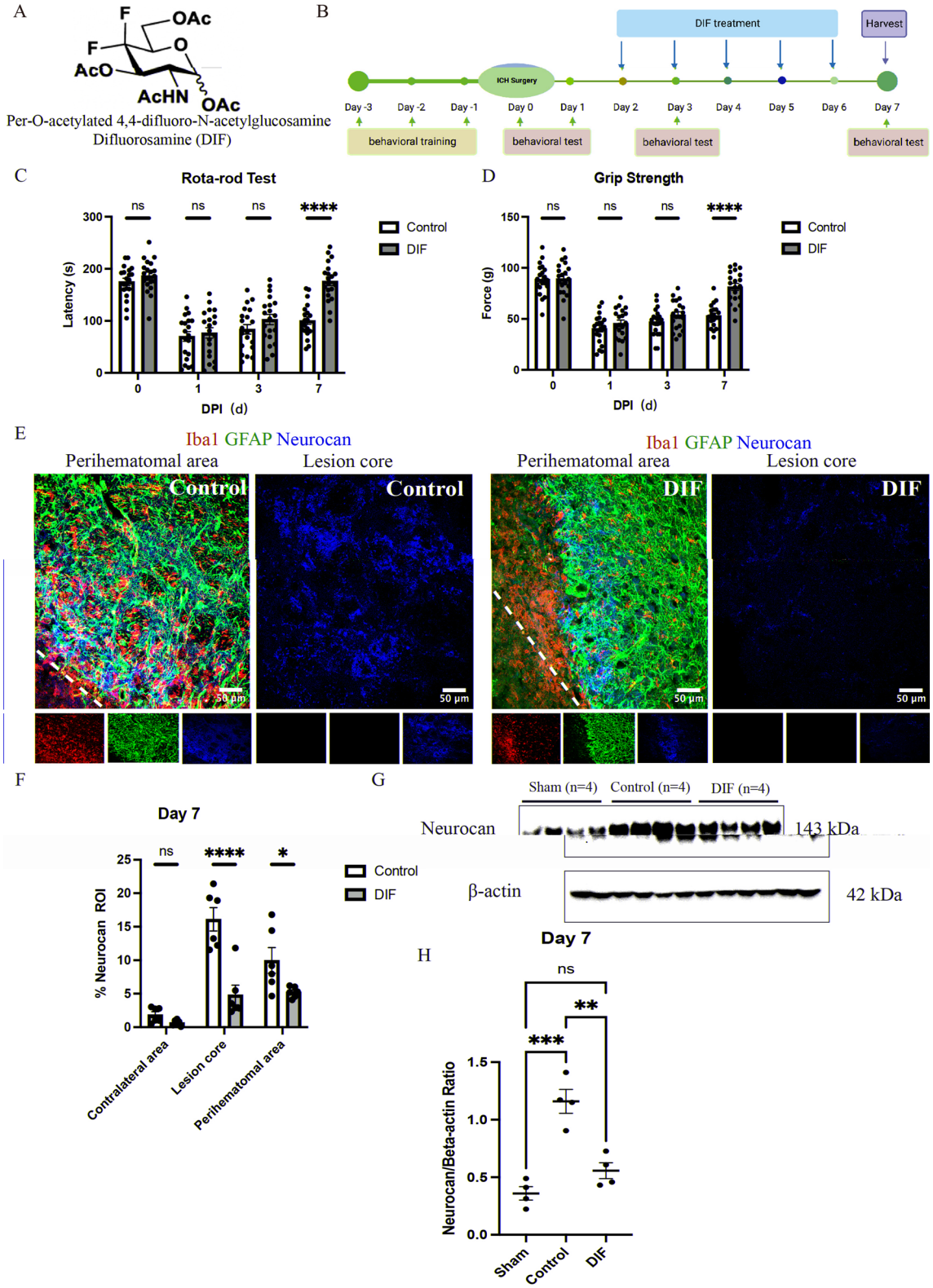

Fig. 2 (See legend on previous page.)

MRI analysis

Using T2-weighted MRI, each ICH lesion and its penumbra was obtained. Briefly, these anatomical images were converted to a common format (NIfTI-1) used in image processing. These images then underwent brain extraction with the 'bet4animal' function implemented in the software FSL (Oxford, UK). The ICH lesions were segmented in 3-dimention (3D) using a lesion-growing method built in the software ITK-SNAP (Penn Image Computing and Science Laboratory). A 3D Penumbral region was derived by dilating the lesion sphere by 2-pixel sizes followed by subtracting from the original segmentation. All lesion volumes were normalized by the brain volume of the corresponding animal.

With diffusion tensor imaging, the 30-direction diffusion-weighted volumes were averaged given their optimal brain-skull contrast per animal to reduce inter-volume variability. The resulting average volumes were used to generate individual mouse brain outlines and brain masks with the 'bet4animal' function of FSL. The prepared diffusion MRI was then processed using the software DSI-studio that included isotropic resampling assisted by the corresponding brain mask obtained above and eddy current correction, among others, to improve data quality. Finally, quantitative analysis of the images allowed to derive four classical DTI measures: fractional anisotropy, mean diffusivity, axial diffusivity, and radial diffusivity.

Eventually, the brain extracted T2 MRI scans were aligned with the FA maps as an example of the diffusion tensor imaging measures through a linear co-registration procedure using FSL to ensure anatomical consistency. Average measurements from 3D lesions or penumbra regions were collected from each diffusion tensor imaging measure of each animal, which were subsequently normalized by the values of their contralateral counterpart obtained by flipping the respective 3D ROIs across the midline.

Statistics

Microsoft Excel (Version 2022 Build 16.69.1) was used for collating data. All graphs were generated using GraphPad Prism 10.0.3. Shapiro–Wilk normality test was applied to verify normal distribution of data. For comparisons between two groups, significance was determined by unpaired two-tailed Student's t-tests for parametric data. Where multiple groups were compared, one/two-way ANOVA with Bonferroni or Tukey's multiple comparison test was used. p values below 0.05 was considered statistically significant shown by asterisks in the figures (*$p < 0.05$, **$p < 0.01$, ***$p < 0.001$, ****$p < 0.0001$). All values are shown as mean ± SEM.

Results

Targeted reduction of neurocan in ICH by AAV-CRISPR/Cas9 promotes oligodendrogenesis and functional recovery

We reported that neurocan elevation after collagenase-induced ICH in mice was apparent at 3 days of injury, peaked at 7 days, and remained elevated in the perihematomal area at 2 weeks [16]. In the current study, we validated ICH lesions at day 7 after collagenase-induced injury through eriochrome cyanine (EC) and neutral red staining, and noted the prominent accumulation of Iba1$^+$ microglia/macrophages and GFAP$^+$ astrocytes at the perihematomal area (Supp. Figure 1A, B). Neurocan was highly expressed in the perihematomal area and lesion core, but not in the contralateral uninjured hemisphere (Supp. Figure 1C–E). Thus, we sought to lower levels of neurocan in astrocytes using CRISPR/Cas9 with GFAP promoter driven SaCas9 and a single guide RNA (sgRNA) targeting exon 4 of the neurocan gene packaged into the PHP.eB serotype of AAV (Supp. Figure 2) in ICH [22], and analyzed functional outcomes over 7 days (Fig. 1A).

AAV knockdown (KD) of neurocan improved the latency before falling in the rotarod test and enhanced forelimb grip strength at day 7 of ICH (Fig. 1B, C). At autopsy, the success of the AAV KD to reduce neurocan levels was corroborated (Fig. 1D, E). Although the AAV was directed to astrocytes, 3D-Imaris surface rendering to better delineate cells showed lower neurocan levels in both GFAP$^+$ astrocytes (Fig. 1F, G) and Iba1$^+$ microglia/macrophages (Supp. Figure 3). Excitingly, AAV reduction of neurocan increased the number of Olig2$^+$ oligodendrocyte lineage cells, olig2$^+$PDGFRα$^+$ OPCs, and

(See figure on next page.)

Fig. 3 Difluorosamine reduces neurocan within microglia/macrophages and shifts their functional state towards a regulatory phenotype. **A** Representative confocal images of perihematomal area at day 7 in control (left) and DIF (right) mice stained for DAPI for cell nuclei (blue) and Iba1 (green). Scale bar = 50 µm. **B** Quantification comparing the number of Iba1$^+$ cells per mm^2 of lesion ROI between control and DIF mice. **C** Representative 3D reconstruction images of perihematomal area at day 7 in control (left) and DIF (right) mice using Imaris rendition, and internal accumulation of neurocan within Iba1$^+$ cells. Scale bar = 5 µm. **D** Bar graphs comparing the percentage of Iba1$^+$ cells containing neurocan molecules between control and DIF mice. **E**, **G**, **I** Representative confocal images of perihematomal area at day 7 in control (left) and DIF (right) mice stained for the indicated markers. Scale bar = 25 µm or 50 µm. **(F**, **H**, **J)** Quantification showing the percentage of IL-1β (**F**), Clec7a (**H**), Arg1 (**J**) in lesion ROI between control and DIF mice. Data are presented as the mean ± SEM of 6 mice. Each dot represents mean of 4 locations per mouse. Unpaired two-tailed Student's *t*-test; ns: not significant. *p < 0.05, **p < 0.01

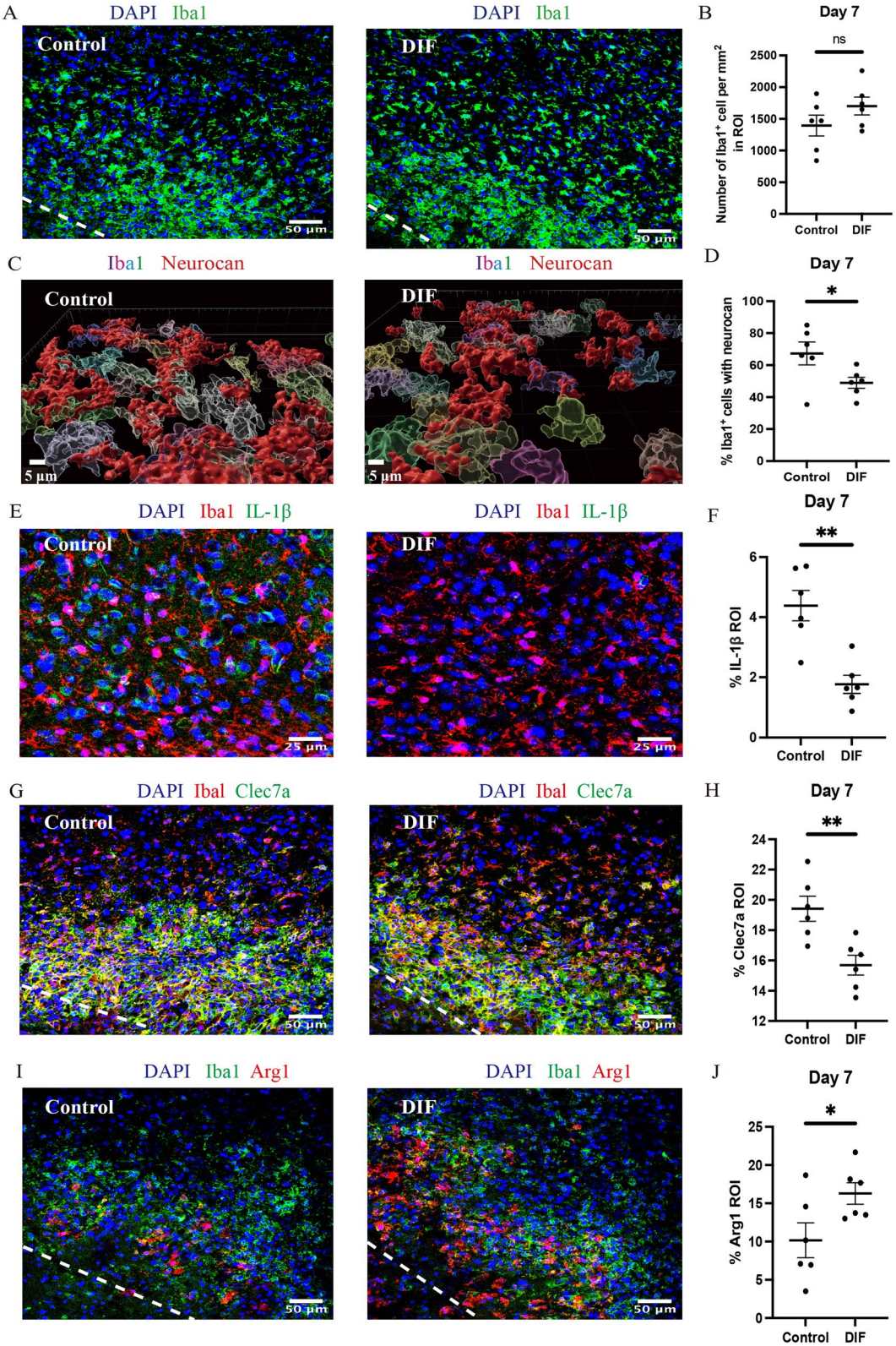

Fig. 3 (See legend on previous page.)

$Olig2^+CC1^+$ mature oligodendrocytes in ICH lesions (Fig. 1H–K).

These results emphasize that the elevation of neurocan in ICH lesions is consequential to inhibiting oligodendrogenesis. Next, we sought a clinically translatable small molecule drug approach to prevent the injury-enhanced deposition of neurocan in ICH.

Daily difluorosamine treatment reduces lesional neurocan and elicits functional recovery over 7 days

Difluorosamine (Fig. 2A) is a potent inhibitor of CSPG biosynthesis [11]. We initiated its daily treatment for 5 days from 2 days post onset of ICH (Fig. 2B). While the initial decline of rotarod and force grip functional activity at days 1 and 3 after ICH was comparable between both groups, indicating similar extent of injury, difluorosamine extended the latency to fall in the rotarod test (Fig. 2C) and enhanced forelimb force of grip strength (Fig. 2D) at day 7. At autopsy, the immunoreactivity for neurocan at lesional regions of interest (ROI) was lowered by difluorosamine (Fig. 2E, F). By corroborative Western blots, the ICH-elevated neurocan was returned to sham levels by drug (Fig. 2G, H). We evaluated whether heparan sulfate proteoglycans were reduced by difluorosamine treatment but could not obtain a clear signal from several antibodies used in Western blots (data not shown). Another ECM protein elevated in ICH, fibronectin, was not affected by difluorosamine (Supp. Figure 4).

Difluorosamine shifts the functional state of microglia/macrophages towards a regulatory phenotype

We determined whether difluorosamine affected $GFAP^+$ and $Iba1^+$ cells in ICH. Difluorosamine treated mice showed reduction of the number of $GFAP^+$ astrocytes (Supp. Figure 4) at 7 days, while there was no change to the number of $Iba1^+$ microglia/macrophages (Fig. 3A, B). The percent of both $GFAP^+$ (Supp. Figure 4) and $Iba1^+$ (Fig. 3C, D) cells with neurocan immunoreactivity was decreased in difluorosamine treated mice compared to control mice.

Although there was no change to the number of Iba1 + microglia/macrophages, their functional properties might have been altered. Pro-inflammatory and damage-associated microglia/macrophages have elevated IL-1β and Clec7a while regulatory cells express arginase-1 (Arg1) [23]. The results show that difluorosamine treatment reduced IL-1β and Clec7a in ROI (Fig. 3E–H), whereas the level of Arg1 was elevated (Fig. 3I, J). Collectively, there appears to be a shift towards regulatory microglia/macrophages upon difluorosamine treatment in ICH.

Difluorosamine improves neurogenesis and oligodendrogenesis after ICH

Enhanced neurogenesis and oligodendrogenesis are observed in divergent CNS pathologies [6, 24]. Given a reduced neurocan load and the shift of microglia/macrophages towards a regulatory state, the lesion after ICH in difluorosamine-treated mice could be more conducive for repair. Indeed, the peri-hematomal area of difluorosamine-treated mice had more $SOX2^+$ and $nestin^+$ neuroblasts, many of which were cycling ($Ki67^+$) (Fig. 4A–E). Similarly, there was also more $Olig2^+$ oligodendrocyte lineage cells, $Olig2^+PDGFR\alpha^+$ OPCs and $Olig2^+CC1^+$ mature oligodendrocytes (Fig. 4F–J).

These results highlight neuroreparative processes including neurogenesis and oligodendrogenesis occurring in neurocan-reduced difluorosamine-treated mice with ICH.

Enhanced oligodendrogenesis also occurs in aging ICH mice after difluorosamine treatment

The prevalence of ICH in humans increases with age, and the prognosis is also worsened [25]. While difluorosamine in the above experiments increased oligodendrogenesis in young mice, it was uncertain whether older subjects would also benefit from the CSPG-lowering drug. We therefore compared the consequence of ICH in young (6-week-old) versus old (52-week-old) mice with ICH, and addressed whether the older age group would also respond to difluorosamine.

Neurocan deposition in the perihematomal area was elevated following injury but the extent was not different between young and aging mice with ICH (young control ICH versus old control ICH) (Supp. Figure 5A, D). The extent of neurocan elevation in the old ICH group

(See figure on next page.)

Fig. 4 Difluorosamine improves neurogenesis and oligodendrogenesis over 7 days of ICH. **A**, **B** Representative confocal images of day 7 perihematomal areas labelled with SOX2 (green), Ki67 (red), nestin (blue) in control (**A**) and DIF (**B**) mice. **C**–**E** Bar graphs comparing number of $SOX2^+$ cells (**C**), $SOX2^+$ $Ki67^+$ (**D**), the percentage of nestin + cells in lesion ROI (**E**). **F**, **G** Representative confocal images of day 7 perihematomal areas labelled with Olig2 (red), PDGFRα (blue), CC1 (green) in control (**F**) and DIF (**G**) mice. The lower left corner inside the dotted lines is the lesion core. Scale bar = 50 µm. **H**–**J** Quantifications comparing number of $Olig2^+$ cells (**H**), OPCs (**I**) or mature oligodendrocytes (**J**) per mm^2 of lesion ROI between control and DIF mice. Data are presented as the mean ± SEM of 6 mice. Each dot represents mean of 4 locations analyzed per mouse. Unpaired two-tailed Student's *t*-test; Significance indicated as $^*p < 0.05$, $^{**}p < 0.01$, $^{***}p < 0.001$

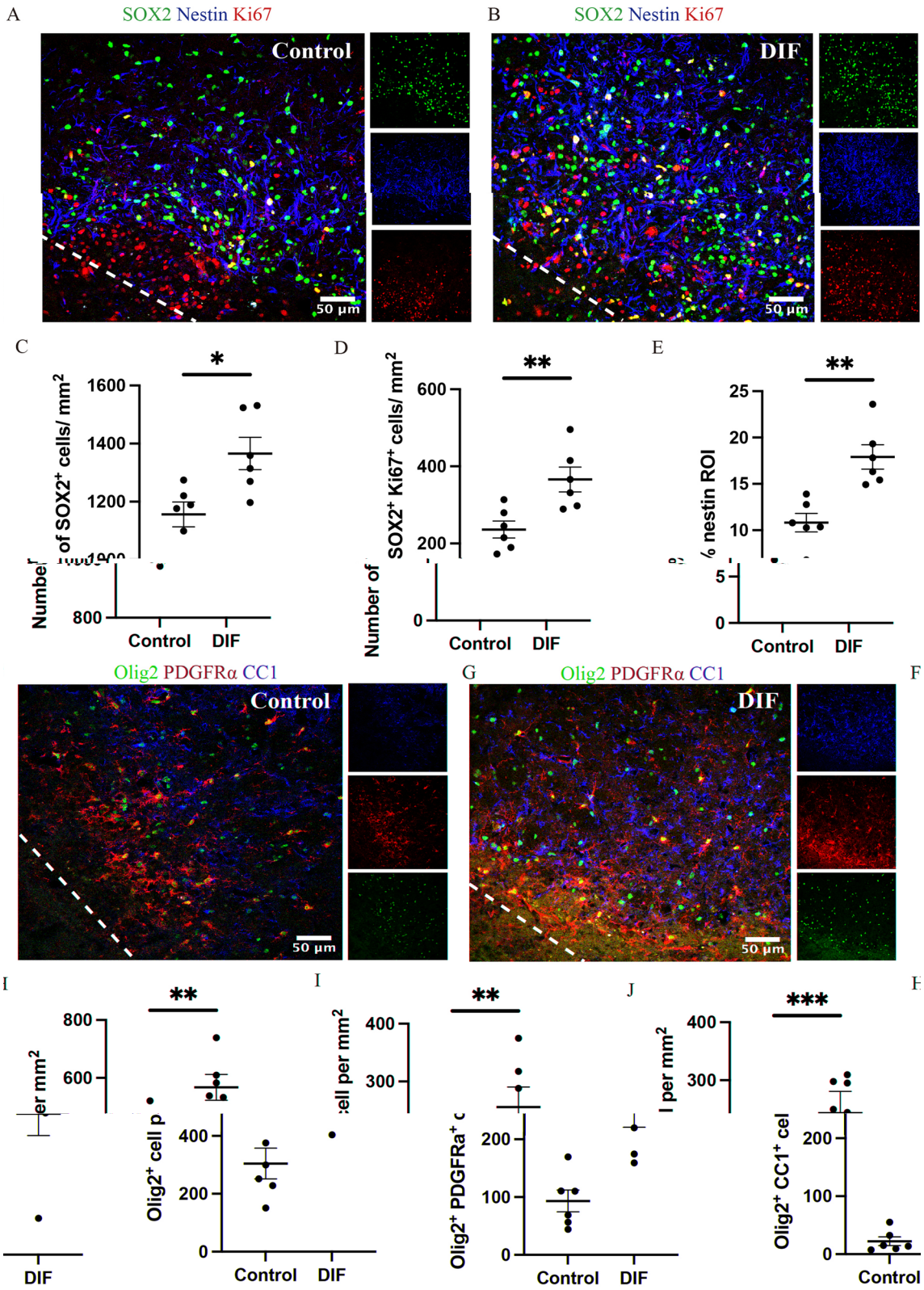

Fig. 4 (See legend on previous page.)

was reduced by difluorosamine treatment (Supp. Figure 5A, D). This was accompanied by elevated numbers of Olig2$^+$PDGFRα$^+$ OPCs and Olig2$^+$CC1$^+$ oligodendrocytes in the perihematomal area (Supp. Figure 5B, C, E–G). These results highlight that difluorosamine is also a pro-regenerative drug in aging mice with ICH.

A protracted alternate day difluorosamine treatment is efficacious over 14 days of ICH

Given that the expression of neurocan remained high at day 14 in the perihematomal region of potentially salvageable tissue [16], we extended the difluorosamine observations and treatment to day 14. Mice were injected IP once every 2 days with difluorosamine or saline from day 3 after ICH (Fig. 5A). Behavioral rotarod and grip force tests ensued before injury, and at days 1, 3, 7 and 14 (Fig. 5A). We found that while the initial decline of rotarod and force grip functional activity was comparable between both groups at days 1 and 3 after ICH (indicating similar extent of injury), difluorosamine alternate day IP injection improved functional recovery that was statistically significant at 14 days (Fig. 5B, C). Brain tissue at day 14 found drug treatment to reduce the level of neurocan immunoreactivity in the perihematomal area (Fig. 5D–F). This was accompanied by difluorosamine-induced switch of microglia/macrophage functional properties from IL-1β+ and Clec7a+ pro-inflammatory and damage-associated myeloid cells to Arginase1$^+$ regulatory cells (Fig. 5G–I) (Supp. Figure 6). Moreover, there was an elevation of SOX2$^+$Ki67$^+$ and nestin$^+$ neuroblasts in the perihematomal area (Fig. 6A–E). The lesion environment was also more conducive for oligodendrogenesis, with increases of Olig2$^+$ oligodendrocyte lineage cells, Olg2$^+$PDGFRα$^+$ OPCs and olig2$^+$CC1$^+$ oligodendrocytes (Fig. 6F–J).

Altogether, these results highlight that difluorosamine treatment reduced neurocan and enhances oligodendrogenesis and neurogenesis over 14 days of ICH.

The efficacy of difluorosamine is corroborated in MRI

Brain MRI imaging was used to analyze ICH lesions and the penumbra regions in response to drug treatment at day 14 both macro- and micro-scopically. Drug was given every other day, from day 3 as described in Fig. 5A. Assisted by robust software tools, all 3D lesion-associated ROIs were successfully segmented (Fig. 7A–C). Between treatment groups, there was no significant difference in normalized lesion volume at day 14 ($p > 0.05$).

Analysis of diffusion tensor imaging (Fig. 7D–G) provided further insight into tissue microscopic characteristics. Specifically, the fractional anisotropy of perihematomal white matter in the striatum of difluorosamine treated mice at day 14 was significantly reduced compared to controls (Fig. 7H). Comparably, the axial diffusivity was significantly decreased in the perihematomal white matter of the treatment group at the same timepoint compared to that of the non-treated group (Fig. 7J). Further, there was a non-significant trend in reduction of mean diffusivity and radial diffusivity (Fig. 7I, K), favoring the treatment group towards tissue recovery or myelin repair. These MRI results corroborate the histological and functional recovery data that difluorosamine improves tissue integrity in the perihematomal area over 14 days of ICH.

Discussion

The microenvironment of ICH lesions is extremely hostile to regenerative processes, as the accumulation of blood/hematoma, proteases and pro-inflammatory molecules constitutes a toxic environment that injures and destroys surviving or regenerating elements [4, 26, 27]. Moreover, debris such as degraded myelin, or neural fragments that persist such as Nogo-A, are not conducive for survival or maturation of cells such as neuroblasts or OPCs, and they inhibit remyelination. Another impediment after ICH is the accumulation of non-permissive ECM [16]. We identified neurocan as the only lectican CSPG member to be prominently elevated in murine and human ICH, but its functional role was inferred from tissue culture experiments where oligodendrocytes seeded onto a purified neurocan substrate had poor adherence and morphological differentiation [16]. Here, we affirmed the negative consequence of neurocan elevation in vivo, by demonstrating that an AAV-CRISPR/Cas9 selective to neurocan results in enhanced oligodendrogenesis and neurogenesis. A clinically translatable inhibitor of

(See figure on next page.)

Fig. 5 Alternate day difluorosamine treatment after ICH promotes functional recovery, reduces neurocan expression and shifts the functional state of microglia/macrophages towards homeostasis over 14 days. **A** Treatment paradigm of difluorosamine in ICH: 14-day experiment. **B**, **C** Bar graphs comparing the latency of rota-rod test (**B**) or forelimb force of grip strength test (**C**) between control and DIF mice. **D**, **E** Representative confocal images of perihematomal area at day 14 in control (**D**) and DIF (**E**) mice stained for neurocan (red), Iba1 (green), GFAP (blue). Scale bar = 50 µm. **F** Bar graphs comparing neurocan percent area of the lesion region of interest (ROI). **G**–**I** Quantification showing the percentage of IL-1β (**G**), Clec7a (**H**), Arg1 (**I**) in lesion ROI between control and DIF mice. Data are presented as the mean ± SEM of 6 mice. Unpaired two-tailed Student's *t*-test; Significance indicated as $^*p < 0.05$, $^{**}p < 0.01$, $^{***}p < 0.001$

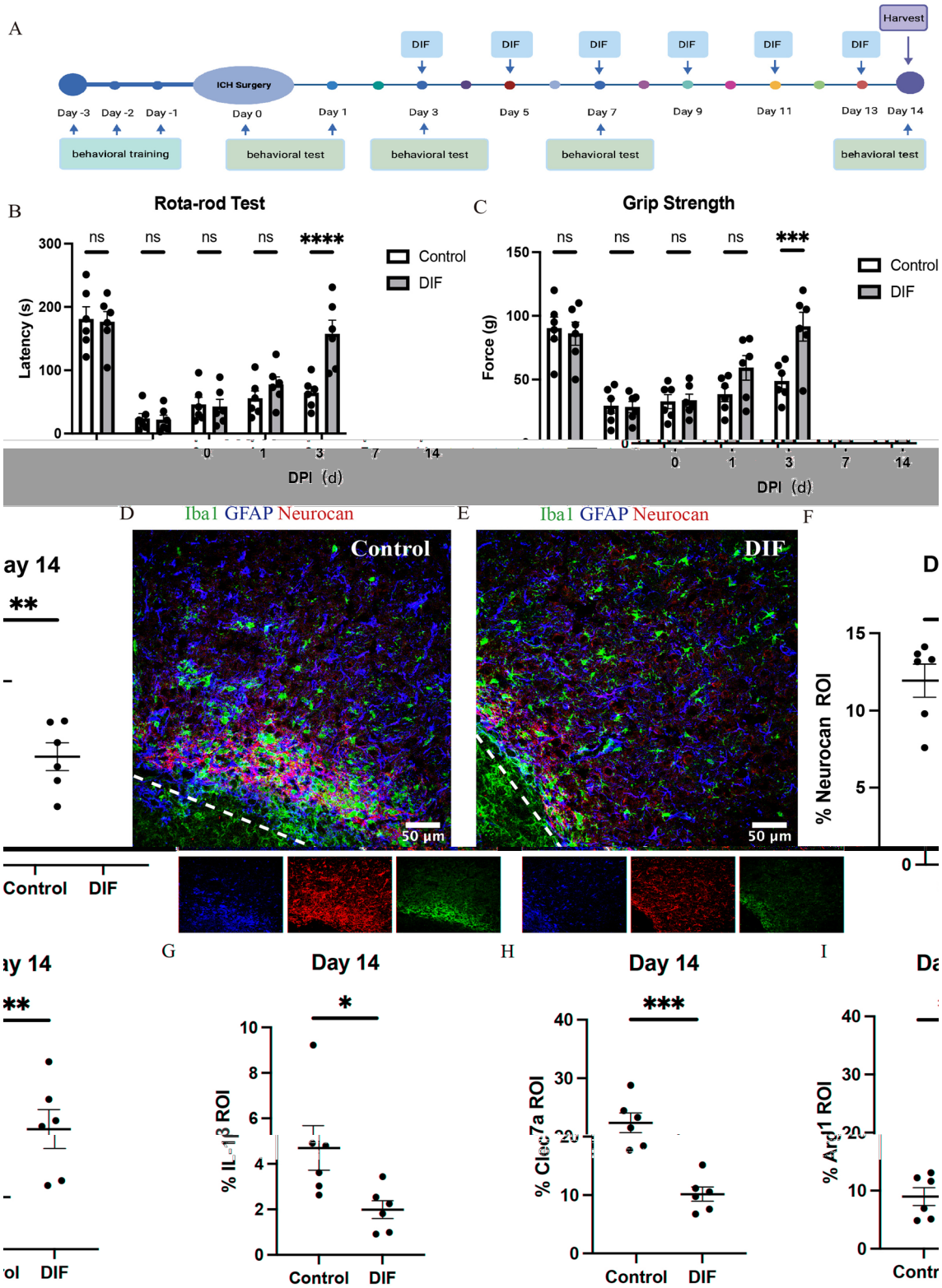

Fig. 5 (See legend on previous page.)

CSPG synthesis, difluorosamine, emphasized neurocan as a particularly important ECM member to overcome in order to improve oligodendrogenesis, neurogenesis and functional recovery after ICH.

While the primary target of difluorosamine is the production of CSPGs, we note that there was some reduction of HSPGs, at least on cultured astrocytes, when the lowering of CSPGs was substantial (Supp. Figure 3 of reference 11). While we sought to document the level of HSPGs in our ICH specimens in the current study, we were unsuccessful in obtaining a Western blot signal when several antibodies to HSPGs were used. Nonetheless, another ECM elevated in ICH specimens, fibronectin, was not affected by difluorosamine (Supp. Figure 4).

The accumulation of CSPGs in CNS lesions across neurological conditions such as traumatic spinal cord injury and multiple sclerosis has been documented for some time [7, 9, 28]. These CSPGs are found to inhibit axonal regeneration and neurogenesis, remyelination, and to promote pro-inflammatory responses [7, 9, 28, 29]. There are several ways that have been undertaken to overcome CSPG detriments in these CNS disorders, including the local application of chondroitinase-ABC to remove the GAG side chains of CSPG [13], and the use of peptides that block the interaction of CSPGs with their receptors such as PTP sigma [30]. We have proposed inhibiting CSPG synthesis by using the fluorosamines [11]. These compounds block the 4-epimerase enzyme and prevent GAG elongation by impeding the conversion of Uridine-5′-diphosphate-*N*-acetyl-D-glucosamine to Uridine-5′-diphosphate-*N*-acetyl-D-galactosamine [11, 31]. While the assembly of GAGs is the primary target, the result of treatment with fluorosamines is the reduction of the whole CSPG (protein core and GAGs) [11].

The literature of how to overcome CSPGs in ICH is sparse. In murine ICH, blocking PTP sigma by intracellular sigma peptide promoted white matter integrity and functional recovery [32]. In premature rabbit pups with intraventricular hemorrhage, chondroitinase ABC treatment reduced the expression of neurocan, but did not enhance maturation of oligodendrocytes, myelination, or neurological recovery [13]. One possible reason is that chondroitinase ABC removes the glycosaminoglycans of CSPGs, but the protein core remains intact and has inhibitory properties.

In the current work, we have tested difluorosamine in ICH, where treatment was initiated at day 2 (in 7-day experiment) or 3 (in the 14-day groups) of ICH when neurocan is beginning to be apparent in lesions [16]. This later treatment initiation avoided the potential role of difluorosamine in affecting the initial lesion evolution. The efficacious effect on oligodendrogenesis and neurogenesis was apparent at 7 or 14 days of ICH (Figs. 4, 6). The difference between short-term and long-term experiments lies in the injection frequency. Daily treatment was administered from day 2 to day 6 for the 7-day ICH, while alternate-day injections were given from day 3 to day 13 for the 14-day ICH. To what extent the fluorosamines cross the blood–brain barrier into the CNS parenchyma from an intraperitoneal injection is not known at this point, but this barrier is often disrupted in neurological conditions.

The favorable histological outcomes after difluorosamine treatment were corroborated by diffusion tensor imaging findings. Brain edema is an important marker of ICH severity and a cause of increased fractional anisotropy during acute and subacute stages following lesion induction in the collagenase animals [33]. Therefore, lower fractional anisotropy in the penumbra regions of difluorosamine-treated than non-treated animals at day 14 may indicate improved recovery in toxic vasogenic edema. On the other hand, lower axial diffusivity in the penumbra of the treated animals likely reflected greater restoration of axonal integrity compared to non-treated subjects. While pending further confirmation, these preclinical MRI results would be instructive in translating our data to clinical trials.

The mechanism of efficacy of difluorosamine in ICH is attributed to its reduction of injury-enhanced neurocan synthesis and deposition into the extracellular matrix. This would remove an inhibitor of oligodendrocyte adhesion and morphological differentiation that we identified in a previous study in culture [16]. Indirect effects could include those on the immune system, as CSPGs have been described to generate pro-inflammatory states of microglia/macrophages [29].

(See figure on next page.)

Fig. 6 Difluorosamine improves neurogenesis and oligodendrogenesis over 14 days of ICH. **A**, **B** Representative confocal images of day 14 perihematomal areas labelled with SOX2 (green), Ki67 (red), nestin (blue) in control (**A**) and DIF (**B**) mice. **C**–**E** Bar graphs comparing number of $SOX2^+$ cells (**C**), $SOX2^+$ $Ki67^+$ (**D**), the percentage of nestin + cells in lesion ROI (**E**). **F**, **G** Representative confocal images of day 14 perihematomal areas labelled with Olig2 (red), PDGFRα (blue), CC1 (green) in control (**F**) and DIF (**G**) mice. The lower left corner inside the dotted lines is the lesion core. Scale bar = 50 µm. **H**–**J** Quantifications comparing number of $Olig2^+$ cells (**H**), OPCs (**I**) or mature oligodendrocytes (**J**) per mm^2 of lesion ROI between control and DIF mice. Data are presented as the mean ± SEM of 6 mice. Each dot represents mean of 4 locations analyzed per mouse. Unpaired two-tailed Student's *t*-test; ns: not significant. Significance indicated as *p < 0.05, **p < 0.01, ***p < 0.001

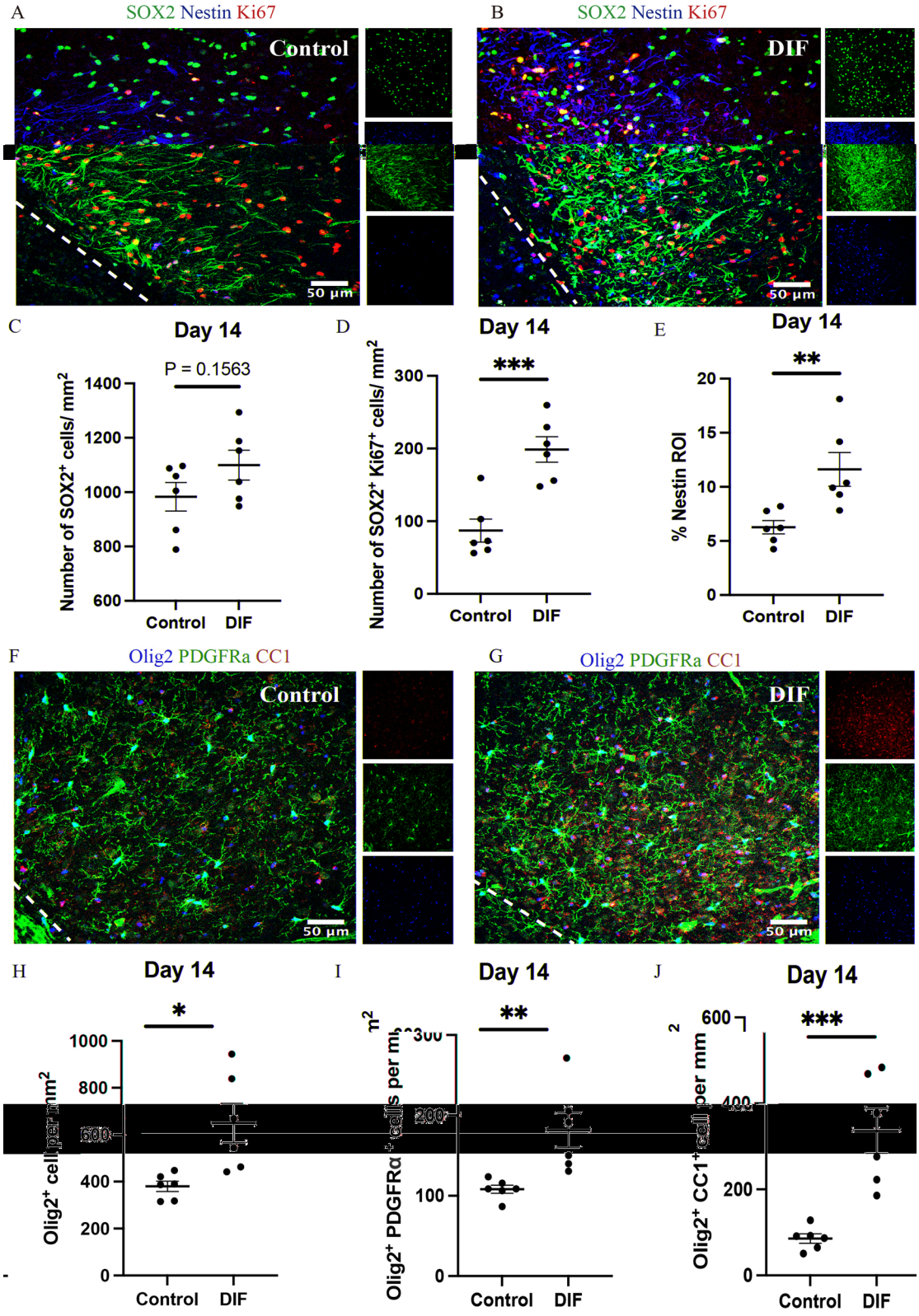

Fig. 6 (See legend on previous page.)

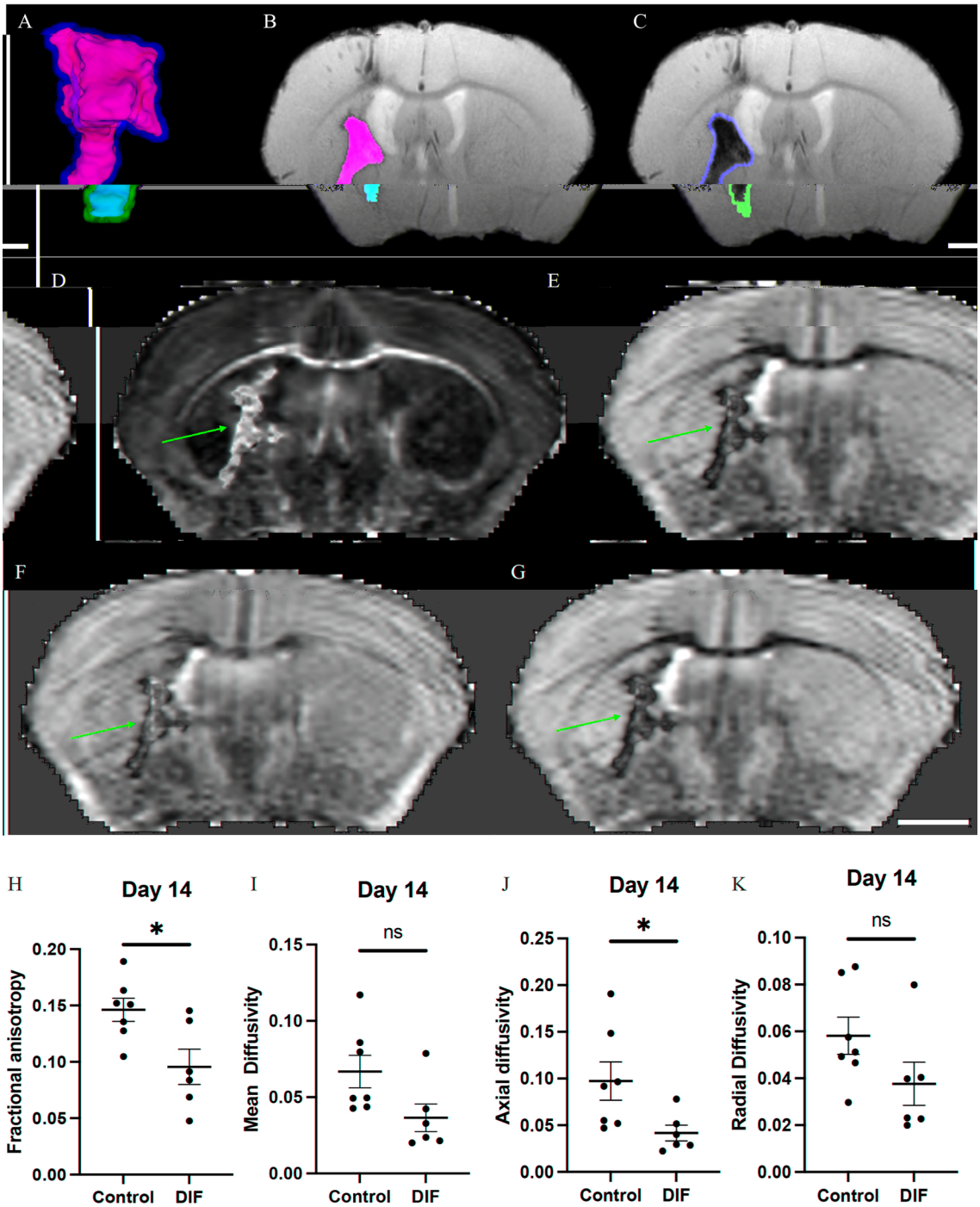

Fig. 7 MRI shows that difluorosamine alleviates brain tissue loss over 14 days of ICH. **A** A 3D representative of segmented perihematomal area and lesion core. **B**, **C** Representative segmented lesion core (**B**) and perihematomal area (blue) (**C**) of FLASH sequences at day 14 after ICH. Scale bar = 3 mm. **D**–**G** Representative images of fractional anisotropy (**D**), mean diffusivity (**E**), axial diffusivity (**F**) and radial diffusivity (**G**) from mice at day 14 after injury. Scale bar = 3 mm. **H**–**K** Bar graphs comparing data from DTI of the perihematomal area between control and DIF mice: fractional anisotropy (**H**), mean diffusivity (**I**), axial diffusivity (**J**) and radial diffusivity (**K**). N = 7 in control group and n = 6 in DIF group. Data are presented as the mean ± SEM. Unpaired two-tailed Student's *t*-test; ns: not significant. Significance indicated as *p < 0.05

Lowering CSPGs with difluorosamine would thus help account for the shift in microglia/macrophage state in our study from degeneration-associated to regulatory in difluorosamine-treated lesions. In studies from single-cell transcriptomics, expression of particular molecules have been broadly classed into functional states of microglia such as pro-inflammatory degeneration-associated (e.g. IL-1β and Clec7a-expressing) or regulatory cells (e.g. arginase expression) (reviewed in 23); the reduced expression of IL-1β and Clec7a, and elevation of arginase in microglia/macrophages in the difluorosamine-treated mice would suggest such a switch of functional states of microglia/macrophages towards regulatory cells. The latter are also more phagocytic [23] and could help clear debris and extravasated blood, and result in the faster resolution of edema that we observed using MRI with difluorosamine. Also, CSPGs have been described to stimulate microglia/macrophage production of matrix metalloproteinases [14], a family of proteases implicated in ICH injury, so reducing CSPG production would likely lead to less matrix metalloproteinases in lesions.

We note that while our primary target in the AAV-CRISPR/Cas9 or difluorosamine experiments is the reduction of neurocan level after ICH, we cannot rule out the possibility that there are secondary effects, such as the reduction of astrocyte number or activity—which we did not assess—that contributed to the observed outcomes. Cells in the CNS influence one another, and an effect on astrocytes could alter oligodendrogenesis.

We did not encounter obvious toxicity of difluorosamine in our ICH study. There was no fatality, and no signs of distress of injected mice. This could be related to the normally low turnover of CSPGs in the CNS, except upon an injury where there is a period of lesion-elevated CSPG synthesis that appears to be blocked by difluorosamine in the current study. If neurocan is initially deposited to help reseal the blood–brain barrier, then immediate treatment after ICH may incur the risk of rebleeding. However, our earliest initiation of difluorosamine was from 48 h after injury, as this was a time point when neurocan deposition in the parenchyma becomes readily apparent by immunofluorescence microscopy, and we did not encounter signs of aggravated injury or rebleeding. Nonetheless, CSPGs do have high turnover in some peripheral tissues such as cartilage joints, so an approach to target difluorosamine into the CNS, such as by the intranasal route or linkage to CNS-targeted formulation, would be an avenue of future study.

Conclusions

In summary, we demonstrate that the reduction of neurocan by AAV-knock down enhanced CNS recovery processes in murine ICH. A small molecule drug, difluorosamine, prevented the rise of injury-enhanced neurocan, and led to favorable lesion outcomes that include neurogenesis, oligodendrogenesis, functional recovery, and better microstructural outcomes on diffusion tensor imaging. We propose the translation of targeting neurocan in ICH with difluorosamine as a new approach to improve recovery from ICH. However, a full toxicological screen would be necessary before undertaking such a transition from preclinical studies into clinical trials.

Abbreviations

AAV	Adeno-associated virus
AD	Axial diffusivity
CNS	Central nervous system
CSPGs	Chondroitin sulphate proteoglycans
DTI	Diffusion tensor imaging
EAE	Experimental autoimmune encephalomyelitis
ECM	Extracellular matrix
FA	Fractional anisotropy
GAG	Glycosaminoglycan
GFAP	Glial fibrillary acidic protein
Iba1	Ionized calcium-binding adapter molecule 1
HRP	Horseradish peroxidase
ICH	Intracerebral hemorrhage
MD	Mean diffusivity
MMPs	Matrix metalloproteinases
OPC	Oligodendrocyte precursor cells
PBS	Phosphate-buffered saline
PFA	Paraformaldehyde
RD	Radial diffusivity
ROI	Regions of interest

Supplementary Information

The online version contains supplementary material available at https://doi.org/10.1186/s12974-024-03331-0.

Supplementary Material 1.

Acknowledgements

We thank the Hotchkiss Brain Institute Advanced Microscopy Platform facility for providing microscopy and image analysis platforms.

Author contributions

H.L. performed most experiments, analyzed the results and wrote the original draft of the paper. S.G. injected the AAV. O.O. and Y.Z. analyzed MRI data. P.Z. and C.L. synthesized and validated difluorosamine. F.V. generated the AAV vectors. J.D. performed MRI imaging. V.W.Y. and M.Z. supervised the study, acquired the funding, edited and finalized the manuscript. All authors reviewed and edited the manuscript.

Funding

This study was funded by the Canadian Institutes of Health Research Grant (No. 1049959) (VWY); the National Key Research and Development Program of China (No. 2018YFC1312200), the National Natural Science Foundation of China (No. 82071331, 81870942, and 81520108011) (MX), and China Scholarship Council (No. 202107040052) (HL).

Availability of data and materials

The datasets used and/or analysed during the current study are available from the corresponding author on reasonable request.

Declarations

Ethics approval and consent to participate
All animal experiments were performed with ethics approval (protocol number AC21-0073) from the Animal Care Committee at the University of Calgary under regulations of the Canadian Council of Animal Care.

Consent for publication
Not applicable.

Competing interests
PZ, CCL and VWY are co-inventors in a US Provisional Patent application (US 63/720,938) titled: Fluorinated glucosamine analogs to reduce injury and promote recovery in neurological disorders.

Author details
[1]Department of Cerebrovascular Diseases, The Second Affiliated Hospital of Zhengzhou University, 2 Jingba Road, Zhengzhou, Henan, China. [2]Hotchkiss Brain Institute and Department of Clinical Neurosciences, University of Calgary, 3330 Hospital Drive, Calgary, AB, Canada. [3]Department of Neurology, Beijing Friendship Hospital, Capital Medical University, Beijing, China. [4]Department of Biology, University of Toronto Mississauga, Mississauga, Canada. [5]Department of Chemistry, University of Calgary, Calgary, Canada. [6]Department of Radiology, University of Calgary, Calgary, Canada.

Received: 17 September 2024 Accepted: 30 December 2024
Published online: 04 January 2025

References

1. Puy L, Parry-Jones AR, Sandset EC, Dowlatshahi D, Ziai W, Cordonnier C. Intracerebral haemorrhage. Nat Rev Dis Primers. 2023;9(1):14.
2. Qureshi AI, Mendelow AD, Hanley DF. Intracerebral haemorrhage. Lancet. 2009;373(9675):1632–44.
3. Sheth KN. Spontaneous intracerebral hemorrhage. N Engl J Med. 2022;387(17):1589–96.
4. Xue M, Yong VW. Neuroinflammation in intracerebral haemorrhage: immunotherapies with potential for translation. Lancet Neurol. 2020;19(12):1023–32.
5. Fu X, Zhou G, Zhuang J, Xu C, Zhou H, Peng Y, et al. White matter injury after intracerebral hemorrhage. Front Neurol. 2021;12: 562090.
6. Uyeda A, Muramatsu R. Molecular mechanisms of central nervous system axonal regeneration and remyelination: a review. Int J Mol Sci. 2020;21(21):8116.
7. Ghorbani S, Yong VW. The extracellular matrix as modifier of neuroinflammation and remyelination in multiple sclerosis. Brain. 2021;144(7):1958–73.
8. Li H, Ghorbani S, Ling CC, Yong VW, Xue M. The extracellular matrix as modifier of neuroinflammation and recovery in ischemic stroke and intracerebral hemorrhage. Neurobiol Dis. 2023;186: 106282.
9. Fawcett JW. The struggle to make CNS axons regenerate: why has it been so difficult? Neurochem Res. 2020;45(1):144–58.
10. Ghorbani S, Jelinek E, Jain R, Buehner B, Li C, Lozinski BM, et al. Versican promotes T helper 17 cytotoxic inflammation and impedes oligodendrocyte precursor cell remyelination. Nat Commun. 2022;13(1):2445.
11. Stephenson EL, Zhang P, Ghorbani S, Wang A, Gu J, Keough MB, et al. Targeting the chondroitin sulfate proteoglycans: evaluating fluorinated glucosamines and xylosides in screens pertinent to multiple sclerosis. ACS Cent Sci. 2019;5(7):1223–34.
12. Zimmermann DR, Ruoslahti E. Multiple domains of the large fibroblast proteoglycan, versican. EMBO J. 1989;8(10):2975–81.
13. Vinukonda G, Zia MT, Bhimavarapu BB, Hu F, Feinberg M, Bokhari A, et al. Intraventricular hemorrhage induces deposition of proteoglycans in premature rabbits, but their in vivo degradation with chondroitinase does not restore myelination, ventricle size and neurological recovery. Exp Neurol. 2013;247:630–44.
14. Stephenson EL, Mishra MK, Moussienko D, Laflamme N, Rivest S, Ling CC, et al. Chondroitin sulfate proteoglycans as novel drivers of leucocyte infiltration in multiple sclerosis. Brain. 2018;141(4):1094–110.
15. Kim S, Takahashi H, Lin WW, Descargues P, Grivennikov S, Kim Y, et al. Carcinoma-produced factors activate myeloid cells through TLR2 to stimulate metastasis. Nature. 2009;457(7225):102–6.
16. Li H, Ghorbani S, Zhang R, Ebacher V, Stephenson EL, Keough MB, et al. Prominent elevation of extracellular matrix molecules in intracerebral hemorrhage. Front Mol Neurosci. 2023;16:1251432.
17. Lau LW, Keough MB, Haylock-Jacobs S, Cua R, Döring A, Sloka S, et al. Chondroitin sulfate proteoglycans in demyelinated lesions impair remyelination. Ann Neurol. 2012;72(3):419–32.
18. Zhang R, Dong Y, Liu Y, Moezzi D, Ghorbani S, Mirzaei R, et al. Enhanced liver X receptor signalling reduces brain injury and promotes tissue regeneration following experimental intracerebral haemorrhage: roles of microglia/macrophages. Stroke Vasc Neurol. 2023;8(6):486–502.
19. Kumar N, Stanford W, de Solis C, Aradhana A, Abraham ND, Dao TJ, et al. The development of an AAV-based CRISPR SaCas9 genome editing system that can be delivered to neurons in vivo and regulated via doxycycline and Cre-recombinase. Front Mol Neurosci. 2018;11:413.
20. Doench JG, Fusi N, Sullender M, Hegde M, Vaimberg EW, Donovan KF, et al. Optimized sgRNA design to maximize activity and minimize off-target effects of CRISPR-Cas9. Nat Biotechnol. 2016;34(2):184–91.
21. Sanson KR, Hanna RE, Hegde M, Donovan KF, Strand C, Sullender ME, et al. Optimized libraries for CRISPR-Cas9 genetic screens with multiple modalities. Nat Commun. 2018;9(1):5416.
22. Challis RC, Kumar SR, Chan KY, Challis C, Beadle K, Jang MJ, et al. Publisher Correction: Systemic AAV vectors for widespread and targeted gene delivery in rodents. Nat Protoc. 2019;14(8):2597.
23. Yong VW. Microglia in multiple sclerosis: protectors turn destroyers. Neuron. 2022;110(21):3534–48.
24. Reuter H, Vogg MC, Serras F. Repair, regenerate and reconstruct: meeting the state-of-the-art. Development. 2019;146(9):dev176974.
25. An SJ, Kim TJ, Yoon BW. Epidemiology, risk factors, and clinical features of intracerebral hemorrhage: an update. J Stroke. 2017;19(1):3–10.
26. Bai Q, Xue M, Yong VW. Microglia and macrophage phenotypes in intracerebral haemorrhage injury: therapeutic opportunities. Brain. 2020;143(5):1297–314.
27. Zhang W, Wu Q, Hao S, Chen S. The hallmark and crosstalk of immune cells after intracerebral hemorrhage: immunotherapy perspectives. Front Neurosci. 2022;16:1117999.
28. Tran AP, Warren PM, Silver J. The biology of regeneration failure and success after spinal cord injury. Physiol Rev. 2018;98(2):881–917.
29. Dyck S, Kataria H, Alizadeh A, Santhosh KT, Lang B, Silver J, et al. Perturbing chondroitin sulfate proteoglycan signaling through LAR and PTPσ receptors promotes a beneficial inflammatory response following spinal cord injury. J Neuroinflamm. 2018;15(1):90.

30. Lang BT, Cregg JM, DePaul MA, Tran AP, Xu K, Dyck SM, et al. Modulation of the proteoglycan receptor PTPσ promotes recovery after spinal cord injury. Nature. 2015;518(7539):404–8.
31. Pu A, Stephenson EL, Yong VW. The extracellular matrix: focus on oligodendrocyte biology and targeting CSPGs for remyelination therapies. Glia. 2018;66(9):1809–25.
32. Yao M, Fang J, Li J, Ng ACK, Liu J, Leung GKK, et al. Modulation of the proteoglycan receptor PTPσ promotes white matter integrity and functional recovery after intracerebral hemorrhage stroke in mice. J Neuroinflamm. 2022;19(1):207.
33. Yang J, Li Q, Wang Z, Qi C, Han X, Lan X, et al. Multimodality MRI assessment of grey and white matter injury and blood-brain barrier disruption after intracerebral haemorrhage in mice. Sci Rep. 2017;7:40358.

Publisher's Note